Evolution of the spin-state transition with doping in $La_{1-x}Sr_xCoO_3$

R. X. Smith, M. J. R. Hoch, W. G. Moulton, P. L. Kuhns, A. P. Reyes, and G. S. Boebinger
National High Magnetic Field Laboratory, Florida State University, Tallahassee, Florida 32310, USA

H. Zheng and J. F. Mitchell
Materials Science Division, Argonne National Laboratory, Argonne, Illinois 60439, USA
(Received 9 December 2011; published 20 August 2012)

The thermally induced spin-state transition of Co^{3+} ions in the cobaltite $LaCoO_3$, found at temperatures in the range 40 to 120 K, has been the subject of extensive experimental and theoretical investigation. Much less is known about what happens to the spin-state transition in hole-doped $La_{1-x}Sr_xCoO_3$ (LSCO). The present ^{139}La NMR experiments show that spin-state transitions persist in nanoscale hole-poor regions of the inhomogeneous doped material. In fact, thermally induced spin-state transitions remain important for doping levels close to the metal-insulator critical concentration of $x_C = 0.17$. This finding suggests that the unusual glassy behavior seen in doped LSCO for $x < 0.18$ results from the interplay of spin-state transitions in hole-poor regions and ferromagnetism in hole-rich regions.

DOI: 10.1103/PhysRevB.86.054428 PACS number(s): 76.60.−k, 75.47.Lx, 75.50.Lk

The hole-doped cobaltite[1] $La_{1-x}Sr_xCoO_3$ evolves with increase in x from a parent insulating compound $LaCoO_3$, in which the Co^{3+} ions undergo a thermally induced spin-state transition across an ∼12 meV energy gap, to become a spin glass at low doping and a ferromagnet at high doping. At the critical doping of $x_C = 0.17$, the system simultaneously undergoes a percolative insulator-to-metal transition (IMT) and a ferromagnetic (FM) order transition. The IMT results from the overlapping of metallic spin clusters that emerge from the close proximity of multiple randomly doped Sr ions.[2,3]

NMR provides a powerful means for detecting local magnetic inhomogeneities from the measured local hyperfine (internal magnetic) field distribution: ^{139}La NMR spectra from single-crystal samples show a doping-dependent distribution of hyperfine couplings consistent with nanoscale phase separation between hole-poor and hole-rich regions.[2,4] We report NMR measurements of spin relaxation rates that reveal the important role of spin-state transitions in hole-poor regions that (1) persist to much higher doping than previously reported from bulk measurements,[5] and can therefore (2) interact with adjacent magnetic clusters.

In the undoped parent compound $LaCoO_3$, spin-state transitions result from the crystal-field splitting of the Co d shell that creates an ∼12 meV gap between the e_g and t_{2g} orbitals. Co^{3+} contains six electrons in its outer d shell that fill the t_{2g} orbitals yielding an $S = 0$ ground state, referred to as the low-spin state. The small crystal-field splitting allows the t_{2g} electrons to be thermally excited into the e_g orbitals and thus a higher-spin state. Current studies seek to determine whether this excited spin state is $S = 1$ or $S = 2$,[6–9] referred to as the intermediate-spin or high-spin state, respectively. Evidence for spin-state transitions comes almost entirely from measurements on the parent compound $LaCoO_3$.

Substituting divalent Sr^{2+} ions for trivalent La^{3+} ions results in spin polarons.[2,10] Neighboring Co ions with mixed valency (Co^{3+} and Co^{4+}) interact ferromagnetically via the double-exchange interaction.[11,12] As doping increases the spin polarons merge and form short-range FM clusters.[2,13,14]

We present high-field ^{139}La NMR spin relaxation measurements that probe the temperature-dependent spin dynamics of $La_{1-x}Sr_xCoO_3$ (LSCO) for a range of doping $0 < x < 0.30$ that spans the spin-glass, IMT, and FM concentration range. We measure a set of floating-zone-grown single-crystal $La_{1-x}Sr_xCoO_3$ samples with $x = 0.05, 0.10, 0.15, 0.18, 0.25$, and 0.30. Measurements on a polycrystalline powder of $x = 0$ were also made. All samples were crushed to a grain size of ∼20 μm to maximize rf penetration into the sample. The ^{139}La ($I = 7/2$; $^{139}\gamma/2\pi = 6.015$ MHz/T) relaxation rate measurements were made with a pulsed NMR spin-echo spectrometer operating at 84.2 MHz in an applied magnetic field of 11–14 T. The hyperfine field (0 to 3 T) at ^{139}La sites in the doped samples acts antiparallel to the applied field. Due to negligible spectral weights at higher temperatures, W_2 and W_1 were measured at only one of two selected points in the spectra corresponding to hyperfine fields of either 0 or 2 T for all dopings except for $x = 0.15$, where it was possible to measure for both fields.

The near-cubic lattice structure yields a transferred hyperfine field, from the eight nearest-neighbor (NN) electron spins on the NN Co ions, at a La nuclear site.[4] The Hamiltonian is $\mathcal{H}_{hf} = \sum_i \mathbf{S}_i \hat{A}_i \mathbf{I}$ with $I = 7/2$ the nuclear spin, $\mathbf{S}_i$ the eight nearest-neighbor electron spins at Co ion sites i, and $\hat{A}_i$ the corresponding transferred hyperfine coupling tensor produced by orbital hybridization. In this work we neglect the small quadrupolar coupling.

The T dependence of the spin-lattice W_1 and spin-spin W_2 relaxation rates for undoped $LaCoO_3$ are shown in Fig. 1(a) while Fig. 1(b) shows these rates for the metallic sample $La_{0.7}Sr_{0.3}CoO_3$. The W_2 dephasing curves are well fitted with a single-exponential function for all dopings while the W_1 relaxation curves exhibit stretched exponential behavior except at the highest temperatures, where they are single exponential. Figures 2(a)–2(e) give the behavior of W_2 with T for x in the range 0.05 to 0.25 at magnetic fields that correspond to the selected hyperfine shifts B_{hf} that are shown in the 4.2 K spectra displayed as insets. The contour plots in the right column of Fig. 2 show the ^{139}La hyperfine field distributions

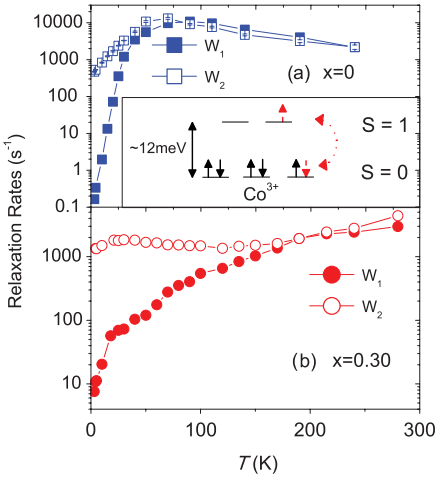

FIG. 1. (Color online) (a) Temperature dependence of W_1 and W_2 measured at a fixed hyperfine field of 0 T for the undoped parent compound $LaCoO_3$. The inset shows the spin-state transition that dominates W_1 and W_2 in the undoped system. (b) W_1 and W_2 measured at a fixed hyperfine field of 2 T for the heavily doped, $x = 0.30$, ferromagnetic system.

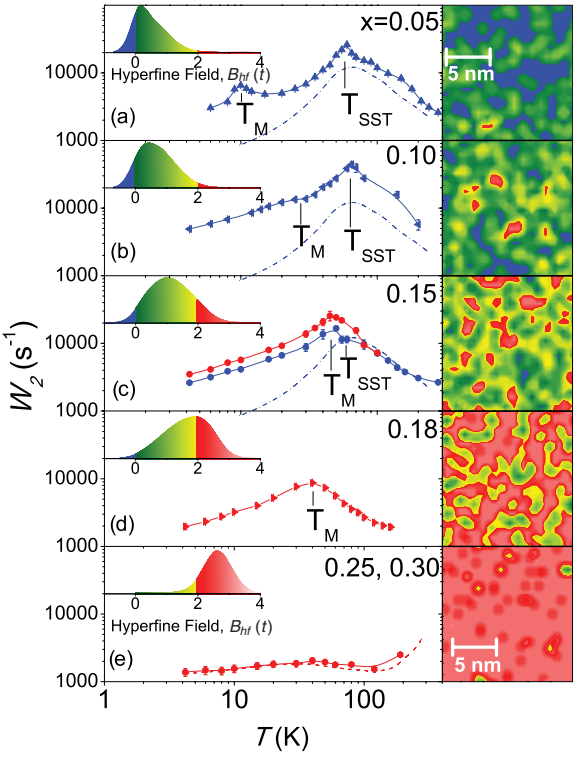

FIG. 2. (Color online) Temperature dependence of the spin-spin relaxation rate W_2 for a range of dopings x, for both hole-poor regions (measured at $B_{hf} = 0$ and shown in blue) and hole-rich regions (measured at $B_{hf} = 2$ T and shown in red). Data for $x = 0$ are plotted as a dash-dotted line in (a)–(c) for comparison. (e) contains data for both $x = 0.25$ and $x = 0.30$ (red circles and dashed line, respectively). The peak T_{SST} at 60 K arises from thermally induced spin-state transitions, which do not change with doping. The T_M peak arises from the critical fluctuations of magnetic ordering in the spin-glass regions. The spectra at the left in each panel show the ^{139}La line shape measured at 4.2 K. The color-coded panels at the right are 2D cross sections of the local moment calculated in a model system from Ref. 2. The color coding from blue (undoped) to red (highly doped) indicates the strength of the internal magnetic field and is common among all measured ^{139}La line shapes and model calculations.

of a two-dimensional (2D) slice of a lattice calculated from the simple statistical model reported in Ref. 2. The contour color mapping correlates to the color mapping under the spectra. The blue areas signify hole-poor regions with very low hyperfine fields (i.e., spectral weight at 0 T arises from nuclei situated in regions of zero electronic-spin polarization) and the red/white regions indicate hole-rich FM regions with high hyperfine fields (>2 T). The green/yellow regions map the intermediate hyperfine field ($0 < B_{hf} < 2$ T) regions that separate the hole-poor and hole-rich regions.

The temperature dependence of W_1 in the parent compound $x = 0$ [Fig. 1(a)] shows a large increase, ~6 orders of magnitude, from 4.2 to 100 K that has been previously explained in terms of spin-state transitions.[15] W_2 for $x = 0$ displays a similar temperature dependence above 60 K as W_1, but experiences only an order of magnitude decrease at low temperature. Both the W_1 and W_2 relaxation mechanisms involve fluctuating hyperfine fields with short correlation times due to thermally induced transitions from $S = 0$ to higher-spin excited states and to spin transitions within the manifold of Zeeman-split excited states. The relaxation rates W_1 and W_2 for the parent compound $LaCoO_3$ in the short-correlation-time limit $\omega_e\tau \ll 1$,

$$W_1 \propto \gamma^2\langle B_\perp^2\rangle\tau, \tag{1}$$

$$W_2 \propto \gamma^2(\langle B_\perp^2\rangle + 2\langle B_\parallel^2\rangle)\tau, \tag{2}$$

where τ is the electronic correlation time describing the electronic spin fluctuations, ω_e the electron Larmor frequency, and $B_\perp$ and $B_\parallel$ the transverse and parallel components of the hyperfine field, respectively. These field quantities are dependent on $\langle S\rangle_{\rm loc}$, the average of the spins S_i on the neighboring Co ions, which has a temperature dependence governed by the spin-state transition.[15] The temperature at the W_2 peak is determined by the crystal-field gap separating the low-spin and higher-spin states. The large difference in the W_1 and W_2 relaxation rates at low temperatures (<20 K) is accounted for as follows. Nuclear dipole-dipole interactions between Co nuclei lead to irreversible dephasing of spins and determine the lower limit of W_2, while no lower limit applies to W_1.

As expected, the relaxation behavior of the $x = 0.30$ FM metallic sample [Fig. 1(b)] is markedly different from that for $x = 0$. For $x = 0.30$, W_1 increases with Korringa-like behavior, $W_1 \propto T$, and W_2 remains roughly temperature independent below the FM ordering temperature $T_C \sim 225$ K.

Figures 2(a)–2(c) show W_2's taken at 0 T hyperfine field (blue regions) for $x = 0$, 0.05, 0.10, 0.15 (open blue circles). The insets show the ^{139}La spectra at 4.2 K reported previously.[2] The main results reported here are the broad peaks at 60 K for $x = 0.05$, 0.10, and 0.15 that reveal the existence of spin-state transitions in hole-poor (blue) regions not apparently detected in other measurements. For $x = 0.05$–0.10 LSCO the maximum in the W_2 vs T plot in Fig. 2 is sharper and somewhat enhanced compared to the values for undoped $LaCoO_3$ (LCO)

which are shown, for comparison, as the dashed curve. The observed differences in the T-dependent behavior of W_2 with x can be qualitatively accounted for as follows. In undoped LCO the local environment of the Co^{3+} ions is different from that in the inhomogeneous doped samples where nanoscale undoped and hole-doped regions coexist as depicted in the color-coded panel in Fig. 2. W_2 at 0 T for $x > 0$ involves contributions from undoped small regions in which the spin gap persists, with associated thermally induced spin-state fluctuations, and from dynamical hole-doped small spin clusters, or spin polarons, with an average static hyperfine field of ~0 T. Evidence for spin-polaron dynamics can be inferred from the T dependence of the ^{139}La LSCO spectra given in Ref. 2. The number of polarons increases with T as large clusters break up and this could lead to a sharpening of the W_2 maximum. The phase-separated dynamical behavior occurs for $0 < x < 0.15$. At $x = 0.15$ the W_2 measurements for hyperfine fields of 0 and 2 T suggest that the spin-polaron contribution is now of dominant importance.

The doped samples exhibit an additional peak, T_M, corresponding to the static ordering of incommensurate short-range spin structures below an ordering temperature $T_I < T_C$ seen by low-temperature elastic neutron scattering.[16] T_M tracks T_I and vanishes by $x = 0.25$, in agreement with the incommensurate spin structures gradually disappearing in the same doping range. T_M and T_{SST} are almost superimposed at $x = 0.15$, near the IMT, suggesting that the value of T_M is regulated by magnetic interactions between hole-poor and hole-rich regions. We point out that these incommensurate structures coexist with hole-rich clusters, in which FM correlations are present. Figures 2(c)–2(e) show W_2 taken at 2 T hyperfine field (red) for $x = 0.15$, 0.18, and 0.25. W_1 and W_2 in the strongly FM metallic samples, $x = 0.25$ and 0.30, exhibit a strong upturn above ~150 K due to spin fluctuations as $T_C \sim 250$ K is approached.

Figure 3(a) shows W_1 taken at 0 T hyperfine field for $x = 0$–0.15. Figure 3(b) shows W_1 taken at 2 T hyperfine field for $x = 0.15$–0.30 (dashed red line). Analogous to the W_2 T-dependent behavior, W_1 at $B_{hf} = 0$ T involves contributions from both spin-state transitions in undoped nanoregions and from dynamical spin-polaron regions. In LSCO for $T < 10$ K, well below the temperature at which spin-state transitions become important, both W_1 and W_2 are much greater than in undoped LCO, consistent with nuclear relaxation induced by fluctuating spin polarons in lightly hole-doped regions. It is likely that for the dynamical polarons $\omega_e\tau > 1$ at the lowest temperatures shown. As mentioned above, the nuclear magnetization recovery exhibits stretched exponential behavior which implies a distribution of relaxation rates in this inhomogeneous material because of the polaron size distribution. As T is raised the magnetic fluctuations enter the fast-correlation-time limit $\omega_e\tau < 1$, resulting in a decrease in nuclear relaxation rates in the polaron environments as given by Eq. (2). Furthermore, the fraction of nuclei at $B_{hf} = 0$ T in the dynamic polaron regions, which have reduced W_1 values, increases as T increases, and this contribution suppresses the measured average W_1. The subsequent upturn in W_1 above ~75 K, where the rates start to approach the $x = 0$ high-T values, corresponds to large-scale melting of spin clusters and coincides with the transition from stretched to single exponential recovery. We note that the transition to a homogeneous distribution of nuclear relaxation rates also coincides with the increasing importance of hyperfine fluctuations arising from thermally induced hole hopping

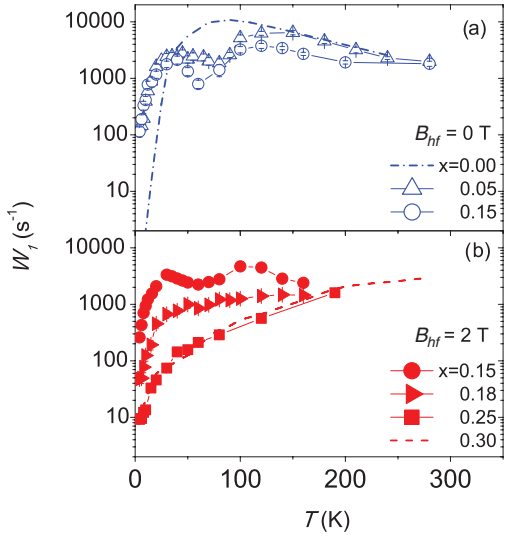

FIG. 3. (Color online) (a) Comparison of the temperature dependence of the spin-lattice relaxation rate W_1 for hole-poor (blue) and hole-rich (red) regions measured at a fixed hyperfine field of 0 T for $x = 0.05$ and 0.15. The dash-dotted line is W_1 for $x = 0$. (b) W_1 measured at a fixed hyperfine field of 2 T for $x = 0.15$, 0.18, 0.25. The W_1 data for 0.30 are plotted as a dashed line. W_1 deviates from $x = 0$ behavior for $x = 0.05$ and $x = 0.15$, whereas W_2 shows little deviation. This indicates a change in the anisotropy of the relaxation mechanisms.

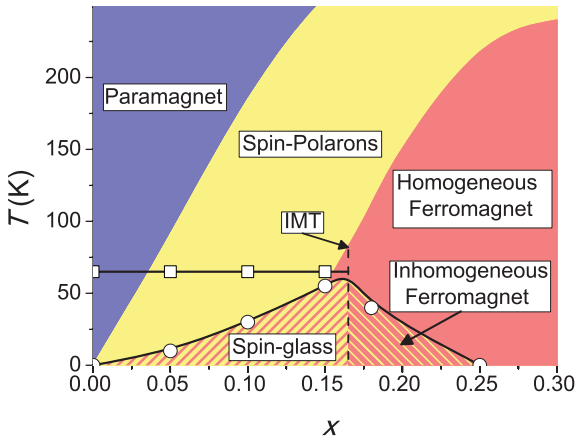

FIG. 4. (Color online) The $La_{1-x}Sr_xCoO_3$ phase diagram. The open squares mark the spin-state transition temperature seen in the hole-poor regions. The open circles and red-yellow hatched areas indicate the magnetic ordered region which agrees with the spin-glass and spin-incommensurate regions seen by susceptibility and neutron scattering measurements. The blue area indicates the region where the system is a paramagnet. The yellow area indicates the region where spin polarons are nucleating around Sr dopants. The red area represents the region where the system exhibits long-range FM order. The boundaries between the colored regions are determined according to NMR measurements (Ref. 2). The dashed vertical line at $x = 0.17$ shows the IMT.

processes which play a role in transport behavior in the insulating material. The electrical conductivity for $x = 0.05$ and $x = 0.15$ LSCO increases for $T > 100$ K.[17]

The main finding of this work is the persistence of spin-state transitions in the hole-poor regions of the doped compounds for x approaching 0.15. The primary experimental evidence for this conclusion is the occurrence of the broad peak T_{SST} in the W_2 data at ∼60 K in Fig. 2 for hole-poor regions ($B_{hf} = 0$ T) of doped LSCO that persists up to $x = 0.15$. This finding is supported by recent theoretical calculations.[18] Hence what has until now been understood to be an insulating spin-glass phase in fact includes the spin-state transitions in hole-poor regions. Figure 4 gives the phase diagram for LSCO based on available information and incorporating the present results. The persistence of spin-state transitions in the insulating phase is shown.

This research is supported by the US Department of Energy Office of Science, Division of Materials Science and Engineering, under Award No. DE-AC02-06CH211357 ("Crystal Growth and Characterization").

[1] J. Wu and C. Leighton, Phys. Rev. B **67**, 174408 (2003).
[2] R. X. Smith, M. J. R. Hoch, P. L. Kuhns, W. G. Moulton, A. P. Reyes, G. S. Boebinger, J. Mitchell, and C. Leighton, Phys. Rev. B **78**, 092201 (2008).
[3] D. N. H. Nam, R. Mathieu, P. Nordblad, N. V. Khiem, and N. X. Phuc, Phys. Rev. B **62**, 8989 (2000).
[4] M. J. R. Hoch, P. L. Kuhns, W. G. Moulton, A. P. Reyes, J. Lu, J. Wu, and C. Leighton, Phys. Rev. B **70**, 174443 (2004).
[5] S. Yamaguchi, Y. Okimoto, and Y. Tokura, Phys. Rev. B **55**, R8666 (1997).
[6] M. W. Haverkort, Z. Hu, J. C. Cezar, T. Burnus, H. Hartmann, M. Reuther, C. Zobel, T. Lorenz, A. Tanaka, N. B. Brookes, H. H. Hsieh, H.-J. Lin, C. T. Chen, and L. H. Tjeng, Phys. Rev. Lett. **97**, 176405 (2006).
[7] M. J. R. Hoch, S. Nellutla, J. van Tol, E. S. Choi, J. Lu, H. Zheng, and J. F. Mitchell, Phys. Rev. B **79**, 214421 (2009).
[8] R. F. Klie, J. C. Zheng, Y. Zhu, M. Varela, J. Wu, and C. Leighton, Phys. Rev. Lett. **99**, 047203 (2007).
[9] D. P. Kozlenko, N. O. Golosova, Z. Jirák, L. S. Dubrovinsky, B. N. Savenko, M. G. Tucker, Y. Le Godec, and V. P. Glazkov, Phys. Rev. B **75**, 064422 (2007).
[10] A. Podlesnyak, M. Russina, A. Furrer, A. Alfonsov, E. Vavilova, V. Kataev, B. Büchner, T. Strässle, E. Pomjakushina, K. Conder, and D. I. Khomskii, Phys. Rev. Lett. **101**, 247603 (2008).
[11] C. Zener, Phys. Rev. **82**, 403 (1951).
[12] P. W. Anderson and H. Hasegawa, Phys. Rev. **100**, 675 (1955).
[13] R. Caciuffo, D. Rinaldi, G. Barucca, J. Mira, J. Rivas, M. A. Señarís-Rodríguez, P. G. Radaelli, D. Fiorani, and J. B. Goodenough, Phys. Rev. B **59**, 1068 (1999).
[14] D. Phelan, D. Louca, S. Rosenkranz, S.-H. Lee, Y. Qiu, P. J. Chupas, R. Osborn, H. Zheng, J. F. Mitchell, J. R. D. Copley, J. L. Sarrao, and Y. Moritomo, Phys. Rev. Lett. **96**, 027201 (2006).
[15] M. J. R. Hoch, P. L. Kuhns, W. G. Moulton, A. P. Reyes, M. A. Torija, J. F. Mitchell, and C. Leighton, Phys. Rev. B **75**, 104421 (2007).
[16] D. Phelan, D. Louca, K. Kamazawa, S.-H. Lee, S. Rosenkranz, M. F. Hundley, J. F. Mitchell, Y. Motome, S. N. Ancona, and Y. Moritomo, Phys. Rev. Lett. **97**, 235501 (2006).
[17] J. Wu, H. Zheng, J. F. Mitchell, and C. Leighton, Phys. Rev. B **73**, 020404 (2006).
[18] A. O. Sboychakov, K. I. Kugel, A. L. Rakhmanov, and D. I. Khomskii, Phys. Rev. B **80**, 024423 (2009).